Acc. Chem. Res. **2000,** *33,* 859−868

Ligand K-Edge X-ray Absorption Spectroscopy: A Direct Probe of Ligand−Metal Covalency

THORSTEN GLASER,† BRITT HEDMAN,*,†,‡ KEITH O. HODGSON,*,†,‡ AND EDWARD I. SOLOMON*,†

Department of Chemistry, Stanford University, Stanford, California 94305, and Stanford Synchrotron Radiation Laboratory, SLAC, Stanford University, Stanford, California 94309

Received April 5, 2000

ABSTRACT

Ligand K-edge X-ray absorption spectroscopy (XAS) is a new experimental probe of the covalency of a metal−ligand bond. The intensity of the ligand pre-edge feature is proportional to the mixing of ligand orbitals into the metal d orbitals. The methodology to determine covalencies in one-electron (hole) and many-electron systems is described and demonstrated for a series of metal tetrachlorides $[MCl_4]^{n-}$, metal tetrathiolates $[M(SR)_4]^{n-}$, and dimeric iron−sulfur (Fe−S) clusters $[Fe_2S_2(SR)_4]^{2-}$. It is then applied to blue Cu proteins, the Cu_A site, hydrogen bonding in Fe−S clusters, and the delocalization behavior in [2Fe-2S] vs [4Fe-4S] clusters. The covalencies determined in these studies provide important electronic structure insight into function.

1. Introduction

1.1. Covalency. Many theories have been developed for understanding the chemical bond. These range from simple principles such as the noble gas configuration, Lewis structures, and qualitative valence bond theory, which have mainly been used in organic chemistry, to crystal field and ligand field theory, mainly used in inorganic chemistry, to the more general molecular orbital (MO) theories used today. Bonding is the degree of interaction between two atoms, which can be described by the amount of covalent mixing of their atomic orbitals. Many concepts in chemistry are based on covalency; therefore, chemists have tried to determine covalency by various spectroscopic methods. In transition metal chemistry, covalency can activate a metal ion and is therefore key for understanding its reactivity. Also, covalency determines magnetic interactions and electron delocalization and thus the physical properties of materials. Many active sites in metalloproteins have a metal−sulfur bond (Figure 1), which governs their electronic structures.[1] Detailed spectroscopic studies, in particular sulfur K-edge XAS, have been successfully applied to understand the electronic structures of these active sites and define this contribution to function. These studies have been accompanied by calculations. Specifically, the recent developments in density functional methods have made it possible to treat larger molecules, including paramagnetic transition metal complexes, at a high level of computation.[2] Experimental methods for determining covalency provide a way to evaluate and calibrate these quantum mechanical calculations.

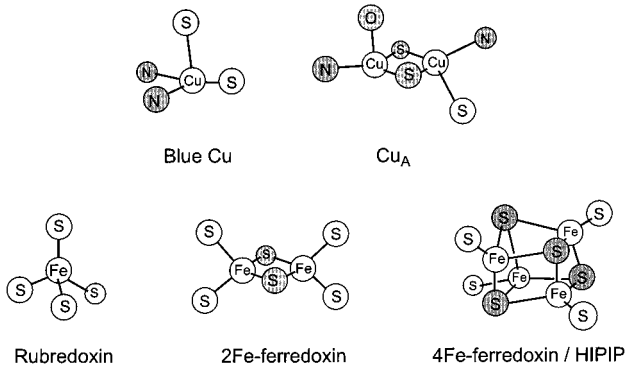

FIGURE 1. Active sites of metalloproteins containing sulfur ligation.

1.2. Traditional Experimental Methods. There are several methods in inorganic chemistry that provide an experimental estimate of the covalency of a metal−ligand bond.[3,4] The methods are based on (1) magnetic measurements of ground-state properties and (2) excited-state and relaxation effects. The first group includes *g*-values, metal hyperfine, and ligand superhyperfine coupling constants obtained from EPR spectroscopy. The second group includes absorption spectroscopy (ligand-to-metal charge transfer, LMCT, and d−d transitions) and photoelectron spectroscopy PES (core and valence level). A summary of these methods as applied to D_{4h}- and D_{2d}-$[Cu^{II}Cl_4]^{2-}$ is given in Table 1. From Table 1, the Cl 3p characters of

Thorsten Glaser was born in Germany in 1970. He received his chemistry diploma in 1995 from the Ruhr-Universität Bochum and was awarded the "Prize for Students of the Ruhr-Universität Bochum" and the "Prize for the best diploma of the Chemistry Department". He obtained his Ph.D. at the Max-Planck-Institut für Strahlenchemie in Mülheim (with K. Wieghardt), focusing on synthesis, and was a postdoctoral fellow at Stanford University, focusing on spectroscopy. He returned to Germany to start his Habilitation at the Westfälische Wilhelms-Universität in Münster to combine these two approaches for the design of new molecular-based magnets.

Britt Hedman was raised in Skellefteå, Sweden. She received her Ph.D. in structural inorganic chemistry in 1978 (with N. Ingri) from University of Umeå, Sweden, where she was Assistant Professor when she in 1985 joined the Department of Chemistry and SSRL, Stanford University, as a Senior Research Associate. She has been an Adjunct Professor of the Department of Inorganic Chemistry, University of Umeå, since 1996. She currently heads the biological X-ray absorption spectroscopy program at SSRL, with her main scientific focus the development and use of XAS for studies of active-site electronic and geometric structure of metalloenzymes as a tool for understanding their function.

Keith O. Hodgson received his Ph.D. in 1972 from the University of California at Berkeley (with K. Raymond and A. Streitwieser, Jr.) and was a NATO-funded postdoctoral fellow at the ETH, Zürich, in 1973 (with J. D. Dunitz and A. Eschenmoser). He was appointed Assistant Professor at Stanford University in 1973, becoming Professor in 1984 and Professor of SSRL in 1992. He became Director of SSRL in 1998. His major scientific interests focus on the development and use of X-ray absorption spectroscopy to investigate the electronic and structural environment of specific metal constituents in noncrystalline macromolecular systems.

Edward I. Solomon grew up in North Miami Beach, FL, received his Ph.D. from Princeton University (with D. S. McClure), and was a postdoctoral fellow at the H. C. Ørsted Institute (with C. J. Ballhausen) and then at Caltech (with H. B. Gray). He was a professor at the Massachusetts Institute of Technology until 1982, when he moved to Stanford University, where he is now the Monroe E. Spaght Professor of Humanities and Sciences. His research is in the fields of physical inorganic and bioinorganic chemistry with emphasis on the application of a wide variety of spectroscopic methods to elucidate the electronic structure of transition metal complexes and its contribution to physical properties and reactivity.

† Department of Chemistry, Stanford University.
‡ Stanford Synchrotron Radiation Laboratory, SLAC, Stanford University.

10.1021/ar990125c CCC: $19.00
Published on Web 09/23/2000

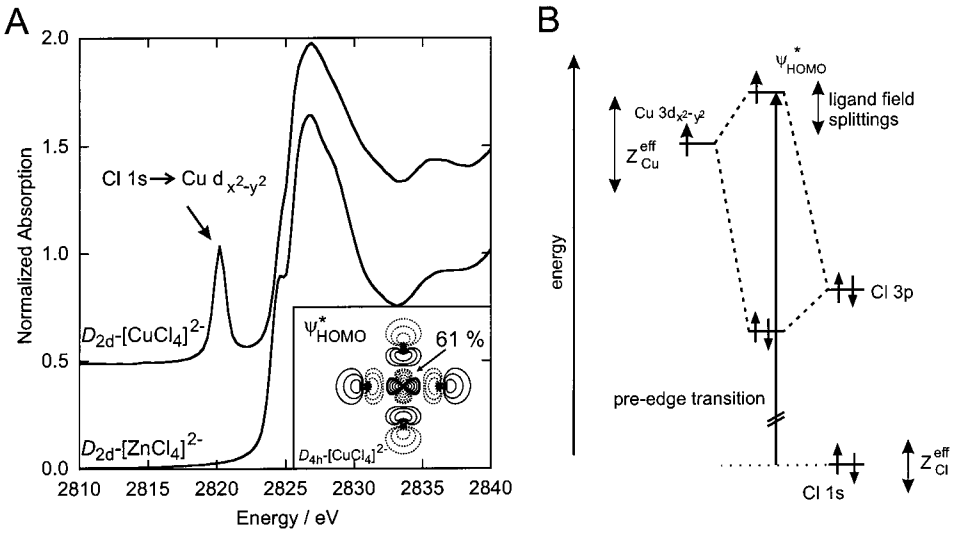

FIGURE 2. (A) Cl K-edge XAS spectra of $[ZnCl_4]^{2-}$ and D_{2d}-$[Cu^{II}Cl_4]^{2-}$; inset shows the $d_{x^2-y^2}$ HOMO of D_{4h}-$[Cu^{II}Cl_4]^{2-}$. (B) Orbital energy diagram showing the ligand pre-edge transition.

Table 1. Experimentally Determined HOMO d Orbital Characters for $[Cu^{II}Cl_4]^{2-}$ [30,31]

method	D_{4h}-$[Cu^{II}Cl_4]^{2-}$	D_{2d}-$[Cu^{II}Cl_4]^{2-}$
g-values, Xα adjusted	61%	71%
copper hyperfine	67%	69%
chloride superhyperfine	64%	75%
d−d and CT energies, configuration interaction model[a]	56%	63%
core level, XPS satellite	60%	68%
valence level, variable energy photoemission	65%	68%

[a] Reference 32.

D_{4h}- and D_{2d}-$[Cu^{II}Cl_4]^{2-}$ are experimentally estimated to be ∼39 ± 5% and ∼30 ± 5%, respectively.

1.3. Ligand K-Edge XAS. The Cl K-edge XAS spectra of the isostructural complexes D_{2d}-$Cs_2[Zn^{II}Cl_4]$ and D_{2d}-$Cs_2[Cu^{II}Cl_4]$ both exhibit an edge jump at ∼2823 eV with a maximum at ∼2827 eV (Figure 2A).[5] Additionally, the copper but not the zinc compound shows an intense low-energy peak at ∼2820 eV. As Zn^{II} has a filled d^{10} electronic configuration, the lowest unoccupied energy levels are the 4s and 4p orbitals. Thus, its edge features derive primarily from the electric-dipole-allowed 1s → 4p transition. Alternatively, Cu^{II} possesses a d^9 electronic configuration with a hole in the d manifold (in the $d_{x^2-y^2}$ orbital for a tetragonal ligand field). The observed pre-edge transition is therefore directly assigned as a Cl 1s → Cu $3d_{x^2-y^2}$ transition (Figure 2B); this transition is not possible in the Zn compound because of the filled d subshell.

Due to the localized nature of the Cl 1s orbital, there can be absorption intensity only if the Cu $3d_{x^2-y^2}$ orbital contains some Cl orbital character. For an electric-dipole-allowed transition, this must be of p type. As shown in Figure 2B, the Cu $3d_{x^2-y^2}$ orbital forms covalent bonds with the Cl 3p orbitals, giving rise to a half-occupied antibonding wave function (eq 1 and Figure 2A inset) with predominantly copper d character. Here, α^2 represents the

$$\psi^*_{HOMO} = (1 - \alpha^2)^{1/2} |\text{Cu } 3d_{x^2-y^2}\rangle - \alpha|\text{Cl } 3p\rangle \quad (1)$$

Cl 3p character in the normalized, symmetry-adapted molecular orbital encompassing the four Cl ligands. The pre-edge transition is therefore more properly described as a Cl 1s → ψ^* transition gaining intensity from the degree of Cl 3p character in the ψ^* wave function. The electric-dipole intensity (Int) is given by eq 2a. Substitution of ψ^* from eq 1 and neglecting all non-one-center integrals results in eq 2b, where const $|\langle \text{Cl } 1s|\mathbf{r}|\text{Cl } 3p\rangle|^2$ is the intensity of a pure, Cl-centered 1s → 3p transition. The

$$\text{Int}(\text{Cl } 1s \rightarrow \psi^*) = \text{const } |\langle \text{Cl } 1s|\mathbf{r}|\psi^*\rangle|^2 \quad (2a)$$

$$= \alpha^2 \text{ const } |\langle \text{Cl } 1s|\mathbf{r}|\text{Cl } 3p\rangle|^2 \quad (2b)$$

intensity of the pre-edge peak is therefore the intensity of a Cl-centered 1s → 3p transition weighted by α^2, the covalent character of the Cl 3p orbitals in the antibonding molecular orbital ψ^*. *Ligand K-edge XAS spectroscopy is therefore a direct probe of the covalency of a metal−ligand bond.*

In this Account, we first give a brief summary of the development of the methodology of ligand K-edge XAS. We then apply this methodology to problems of bioinorganic relevance.

2. Methodology

2.1. Theoretical Aspects. A more complete derivation of eq 2 is presented in ref 6. The comparison between the LMCT observed in electronic absorption spectra of transition metal complexes and the pre-edge transition of ligand K-edge XAS is instructive. LMCT involves the transition of an electron from a bonding MO with both metal and ligand character to an antibonding MO also with both metal and ligand character. This gives rise to an intense, electric-dipole-allowed absorption band in the UV/vis region of transition metal spectra. Formally, a ligand pre-edge absorption feature can also be viewed as a LMCT, involving a transition of an electron from a ligand 1s orbital to an antibonding MO with both metal and ligand character. However, in this case the donor orbital has only

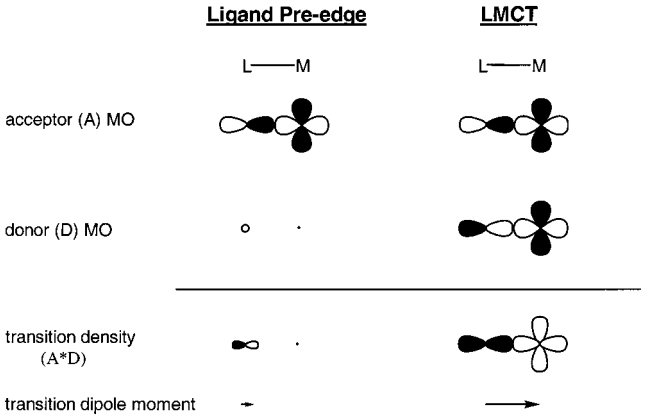

FIGURE 3. Comparison of the electric dipole intensity mechanism for a ligand pre-edge XAS transition and a LMCT. The transition density is localized on the ligand in the pre-edge transition, whereas the transition density goes from the ligand toward the metal in the LMCT. This is indicated by the arrows at the bottom of the figure.

ligand character because the contracted ligand 1s orbitals have no overlap with metal orbitals. The transition dipole moment is therefore localized on the ligand, whereas for a LMCT the transition dipole moment is directed from the ligand to the metal (Figure 3).[6] This results in a bond length dependence of an LMCT but not for a ligand pre-edge transition.

The intrinsic, localized ligand 1s → ligand np transition dipole moment depends on the effective nuclear charge of the ligand, Z^{eff}, which governs the radial distribution of the np orbitals.[7] A second factor influencing the intrinsic transition moment is covalent bonding, which redistributes np electron density into the region between the ligand and the metal. Calculations show that the charge dependence of the transition dipole moment is relatively small over the range that Z^{eff} is expected to change in transition metal complexes.[6]

Final state relaxation of ligand orbitals could give rise to differences in the metal−ligand bonding relative to the ground state, which would complicate the analysis of ligand pre-edges. This phenomenon is well known from metal K- and L-edge XAS, and XPS where a metal core hole is created.[8,9] The relaxation leads to shake-up transitions, which are formally forbidden two-electron transitions. These involve the creation of a core hole and a LMCT transition to compensate for the increased positive charge on the metal. The absence of shake-up intensity in ligand K-edges indicates that final state relaxation is not significant. This is corroborated by MO calculations which show that there are no efficient relaxation pathways for donor ligands.[6]

2.2. d^9 Systems: Energy and Intensity of the Pre-edge. As indicated in Figure 2B, three factors affect the energy position of a ligand pre-edge transition. A chemical shift in the ligand 1s core energy, which is related to the effective charge on the ligand, changes the pre-edge energy. Similarly, delocalization of ligand electron density onto the metal due to bonding results in a core orbital shift to deeper binding energy. Since the unoccupied ligand 4p orbitals are less affected by charge donation,

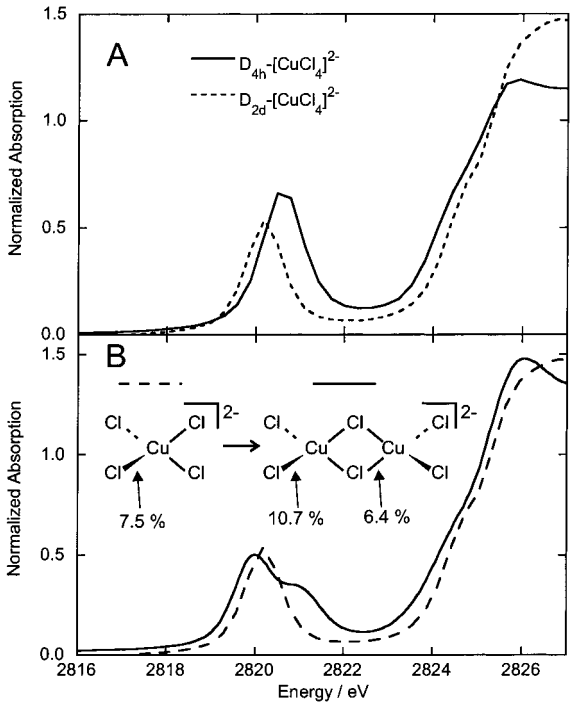

FIGURE 4. (A) Comparison of the Cl K-edge XAS spectra of D_{2d}-$[Cu^{II}Cl_4]^{2-}$ and D_{4h}-$[Cu^{II}Cl_4]^{2-}$. (B) Comparison of the Cl K-edge XAS spectra of D_{2d}-$[Cu^{II}Cl_4]^{2-}$ and $[Cu_2Cl_6]^{2-}$.[5]

shifts in the energies of the rising edge directly reflect shifts in the ligand 1s core.

In addition, the energy of a ligand pre-edge transition is affected by the HOMO energy, which has two major contributions: (1) the geometry of the ligand field of the complex determines the d orbital energy splitting pattern and (2) the overall d manifold can shift in energy. This is related to both the coordination number of the metal (the total antibonding and repulsive interactions with the ligands) and Z^{eff} of the metal, which affects the energy of all metal orbitals.

The comparison of the Cl K-edges of D_{2d}- and D_{4h}-$[Cu^{II}Cl_4]^{2-}$ illustrates the different effects on the energies of a ligand pre-edge transition (Figure 4A).[10] The pre-edge peak in D_{4h}-$[Cu^{II}Cl_4]^{2-}$ occurs at 2820.6 eV and in D_{2d}-$[Cu^{II}Cl_4]^{2-}$ at 2820.2 eV. The rising edge positions[11] are 2825.0 and 2825.3 eV, respectively, which indicates that the Cl 1s core level in D_{2d}-$[Cu^{II}Cl_4]^{2-}$ is 0.3 eV deeper in binding energy than in the D_{4h}-isomer. This implies a higher Z^{eff} of the chloride ligands in D_{2d}-$[Cu^{II}Cl_4]^{2-}$, indicating more *total* charge donation of the chlorides to the copper ion. This should shift the pre-edge up in energy, yet it is lower than that for D_{4h}-$[Cu^{II}Cl_4]^{2-}$ by 0.4 eV. This has two contributions: ligand field effects and Z^{eff} of the copper. The shift of the HOMO due to ligand field effects can be estimated through an analysis of the ligand field transitions of these complexes (0.9 eV).[10] Correcting for this contribution yields the HOMO shift due to an overall change of the d manifold binding energy. This analysis results in a +0.2 eV higher lying d manifold for D_{2d}-$[Cu^{II}Cl_4]^{2-}$, indicating a lower Z^{eff} for the Cu^{II} in this geometry. This is consistent

with the increased charge donation of the chloride ligands from the energy of the Cl K-edge.

To convert the experimentally determined intensities into covalencies, the value of the transition dipole moment integral is needed (eq 2b). Using 39% Cl character in D_{4h}-$[Cu^{II}Cl_4]^{2-}$ (Table 1, left), i.e., ~10% per bond, to calibrate the intensity of the pre-edge in Figure 4A, the intensity of the D_{2d}-$[Cu^{II}Cl_4]^{2-}$ pre-edge gives 30% covalency (eq 2), i.e., ~7.5% per bond.[12] This is in agreement with the results of other methods in Table 1 and derives from the better overlap of the Cl 3p orbitals with the $d_{x^2-y^2}$ orbital in D_{4h}-$[Cu^{II}Cl_4]^{2-}$, where the lobes point directly at the Cl ligands. Thus, even though the HOMO for the D_{4h} complex has a higher covalent contribution from the chloride ligands, the distortion from planarity in D_{2d}-$[Cu^{II}Cl_4]^{2-}$ allows a more favorable total bonding interaction over the five d orbitals between the chlorides and the copper.

2.3. Dimeric d^9 Systems: Terminal and Bridging Ligands. The differences between the spectra of monomeric and dimeric compounds are demonstrated in Figure 4B, which shows the Cl K-edge spectra of D_{2d}-$[Cu^{II}Cl_4]^{2-}$ and the tetrahedral dimer $[Cl^t_2Cu^{II}(\mu_2\text{-}Cl^b)_2Cu^{II}Cl^t_2]^{2-}$.[10] The single pre-edge peak of the monomer is split into two peaks, a weaker peak shifted 0.9 eV to higher energy and a more intense peak shifted 0.2 eV to lower energy. The assignment of the two peaks is straightforward considering that the transition from the 1s of the terminal Cl^t and of the bridging Cl^b is to the same HOMO of the copper ions. Therefore, the energy separation reflects the difference in Cl 1s binding energies. The bridging ligand donates charge to two copper centers, leading to a higher Z^{eff} and a deeper 1s binding energy. The higher energy peak is therefore assigned to a transition of the bridging ligand and the lower energy peak to a transition of the terminal ligand. Analysis of the peak intensities (renormalized for 2 Cl^b vs 4 Cl^t) gives a covalency of 10.7% and 6.4% per metal–ligand bond for the terminal and bridging chlorides, respectively. It is now insightful to compare the nonbridging (terminal) chloride ligands of this dimer to the equivalent chloride ligands of the tetrahedral D_{2d} monomer (Figure 4B). These ligands are not changed on going from the monomer to the dimer and can therefore be used as spectator ligands which reflect changes of the electron density at the copper center upon changing two nonbridging ligands to μ_2-bridging ligands. Comparison of the covalencies of the terminal chlorides between the monomer (7.5%) and the dimer (10.7%) shows the effect of the poorer charge donation per bond of the bridging chloride and its compensation by increased charge donation from the terminal ligands. Thus, these terminal chlorides function as spectator ligands for the electron density at the copper center.

2.4. d^n Metal Ions: The Metal Tetrachloride Series. The ligand K-edge XAS spectra of a series of tetrahedral metal tetrachlorides $[MCl_4]^{2-}$ all exhibit a pre-edge feature in the 2820–2824 eV range (Figure 5A).[7] Over the divalent series, the energies of the pre-edge features vary in the order $Cu^{II} < Ni^{II} < Co^{II} < Fe^{II}$; the pre-edge of $[Fe^{III}Cl_4]^-$ is shifted 2.3 eV to lower energy compared to that of

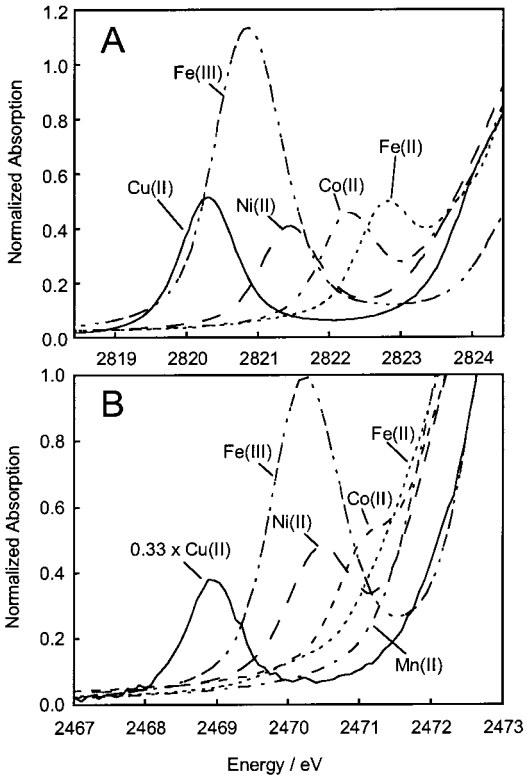

FIGURE 5. (A) Pre-edge region of the Cl K-edge XAS spectra of the T_d complexes $[MCl_4]^{n-}$, with M = Cu^{II}, Ni^{II}, Co^{II}, Fe^{II}, and Fe^{III}.[7] (B) Pre-edge region of the S K-edge spectra of the S_4 complexes $[M(SPh\text{-}2\text{-}Ph)_4]^{n-}$, with M = Ni^{II}, Co^{II}, Fe^{II}, Mn^{II}, Fe^{III}, and plastocyanin (Cu^{II}).[14] The intensity of plastocyanin is scaled down by one-third.

$[Fe^{II}Cl_4]^{2-}$. The rising edge energy positions in the spectra are all very close to 2825 eV, except that for Fe^{III} which is at 2826 eV. The pre-edge feature of $[Cu^{II}Cl_4]^{2-}$ is more intense than those of the other divalent complexes, which are nearly identical, while the pre-edge of $[Fe^{III}Cl_4]^-$ is 3 times more intense.

The trend in the energy position of the pre-edge features over the divalent series reflects the energy diagram in Figure 2B. As described in section 2.2., there are three main contributions to the pre-edge energy. The nearly identical energy of the rising edge inflection point corresponding to the Cl 1s energy indicates that a change of Z^{eff} on the chlorides is not responsible for the large shift of the pre-edge energies. The excited-state ligand field splittings are on the order of 2 eV, varying only by a few tenths of an electronvolt over the series. Therefore, the main contribution to the pre-edge energy shift is the change in Z^{eff} of the metal ion, which increases in the order $Fe^{II} < Co^{II} < Ni^{II} < Cu^{II}$, in agreement with the expected trend on going from left to right in the periodic table. The 2.3 eV decrease in pre-edge energy on going from Fe^{II} to Fe^{III} mainly reflects the increased Z^{eff} due to oxidation of the iron center.

The relationship between the intensity of the pre-edge peak of a ligand K-edge XAS spectrum and the covalency described above for transition metal ions with a d^9 electron configuration is straightforward because there is only one possible parent configuration (d^{10}) in the final

Table 2. Strong Field Dipole Strength Expressions for $[MCl_4]^{n-}$ Pre-edge Transition Intensities and Total Covalencies[a]

complex	dipole strengths, D_0	total covalency = $(3D_0/\langle s\|\mathbf{r}\|p\rangle^2)$
$[Cu^{II}Cl_4]^{2-}$	$^1/_3(c_1^2 + c_2^2)\langle s\|\mathbf{r}\|p\rangle^2$	$(c_1^2 + c_2^2)$
$[Ni^{II}Cl_4]^{2-}$	$^2/_3(c_1^2 + c_2^2)\langle s\|\mathbf{r}\|p\rangle^2$	$2(c_1^2 + c_2^2)$
$[Co^{II}Cl_4]^{2-}$	$(c_1^2 + c_2^2)\langle s\|\mathbf{r}\|p\rangle^2$	$3(c_1^2 + c_2^2)$
$[Fe^{II}Cl_4]^{2-}$	$(c_1^2 + c_2^2 + {}^1/_3c_3^2)\langle s\|\mathbf{r}\|p\rangle^2$	$3(c_1^2 + c_2^2) + c_3^2$
$[Fe^{III}Cl_4]^{-}$	$(c_1^2 + c_2^2 + {}^2/_3c_3^2)\langle s\|\mathbf{r}\|p\rangle^2$	$3(c_1^2 + c_2^2) + 2c_3^2$
general	$((h_{t_2}/3)(c_1^2 + c_2^2) + (h_e/3)c_3^2)\langle s\|\mathbf{r}\|p\rangle^2$	$h_{t_2}(c_1^2 + c_2^2) + h_e c_3^2$

[a] c_1^2, σ-covalency in the t_2 set; c_2^2, π-covalency in the t_2 set; c_3^2, π-covalency in the e set.

state. In systems with more than one d manifold hole, transitions to more than one partially occupied metal d-derived orbital are possible, each producing several many-electron excited states. Further, multiplet effects in the d^{n+1} excited state can redistribute the observed intensity. Therefore, a methodology to analyze the pre-edge intensity for the determination of covalency, which takes into account all of these contributions, was developed.[7]

The methodology presented in ref 7 involves (1) determination of electric-dipole-allowed pre-edge transitions, (2) derivation of dipole strength expressions for these allowed strong field transitions using the irreducible tensor method, and (3) consideration of mixing of excited states in intermediate ligand fields, which can redistribute pre-edge intensity to higher energy. To extract information about ligand−metal covalency, the intensity of these pre-edge transitions between many-electron ground and final states must be related to the amount of ligand 3p character in the one-electron t_2 and e orbitals.

The resulting total dipole strength expressions in the strong field limit are summarized in Table 2. Here, $\langle s|\mathbf{r}|p\rangle^2$ is the intensity of a pure Cl 1s → Cl np transition. The dipole strength expressions can be generalized to the relation given at the bottom of Table 2, where h_{t_2} and h_e are the number of holes in the t_2 and e manifolds, respectively, and c_1, c_2, and c_3 are the σ-covalency of the e set and the σ- and π-covalency of the t_2 set, respectively.[13] This dipole strength expression can also be applied to octahedral complexes considering σ interactions with the e_g set and π interactions with the t_{2g} set. Multiplying the dipole strength by $3/\langle s|\mathbf{r}|p\rangle^2$ gives the *total covalency* (the sum of the individual covalencies of all half-occupied or unoccupied molecular orbitals) for *all* electron configurations.

The relative pre-edge intensities of $[MCl_4]^{2-}$ in Figure 5A are 6:4:4:4 for Cu^{II}:Ni^{II}:Co^{II}:Fe^{II}. Three contributions lead to this intensity pattern. (1) The pre-edge intensity is related to the statistical probability of an allowed pre-edge transition. The dipole strength expressions in Table 2 for Cu^{II}:Ni^{II}:Co^{II}:Fe^{II} predict an intensity ratio of 1:2:3:4 (everything else being equal), in proportion to the number of d holes in the ground state. (2) The pre-edge intensity is reduced by configurational mixing with higher energy states (29% and 16% for $[Fe^{II}Cl_4]^{2-}$ and $[Co^{II}Cl_4]^{2-}$, respectively[7]), but this still does not give the observed intensity ratio. Therefore, the final contribution (3) to the pre-edge intensity reflects the covalency of the metal−ligand bond. While the statistical probability of a pre-edge transition increases, the covalency decreases across the series from Cu^{II} to Fe^{II}. Additionally, the π-covalency of the e orbitals is less than the covalency of the t_2 orbitals, which further decreases the intensity of Fe^{II}. Experimental estimates for the covalencies are given in Table 3 and compared to the results of DFT calculations. The high intensity of $[Fe^{III}Cl_4]^{-}$ in Figure 5A reflects 86% total covalency or 21.5% per Fe^{III}−Cl bond.

Table 3. Comparison of Covalencies Per Metal−Ligand Bond in the Tetrachloride and Tetrathiolate Series[b]

	$[MCl_4]^{n-}$	Xα	$[M(SR)_4]^{n-}$
Cu^{II}	7.5%	7.0%	38% (plastocyanin)
Ni^{II}	6.1%	8.3%	16.4% (SR = SPh-2-Ph)
Co^{II}	7.1%	9.2%	14.2% (SR = SPh-2-Ph)
Fe^{II}	8.6%	9.3%	20%[a] (SR = SPh)
Fe^{III}	21.5%	26.4%	38.4% (SR = SPh)

[a] Due to overlap of the pre-edge feature with the rising edge, the fitting of the pre-edge does not yield unique solutions. Therefore, the value given above is determined through correlation of experimental to calculated trends.[17,28] [b] Note that the covalency values differ relative to those reported in refs 7 and 14, which included an R^2 factor in the equations in Table 2.

Chart 1

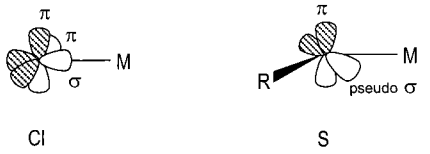

2.5. The Metal Tetrathiolate Series: The RS^-—M bond. To study metalloproteins with cysteine ligation, the study of ligand K-edge XAS was expanded to a series of metal tetrathiolates $[M(SR)_4]^{n-}$ with M = Mn^{II}, Fe^{II}, Co^{II}, Ni^{II}, and Fe^{III} (Figure 5B);[14] the S K-edge of plastocyanin (Cu^{II}) is used as a reference (see section 3.1.). The presence of the thiolate group leads to a reduction of the symmetry of the complexes (S_4) and to anisotropic covalency. While one of the three valence p orbitals of chloride is used for σ-bonding to the metal and the other two for π-bonding, in thiolates one sulfur p orbital is mainly involved in the strong S−C bond. For the generally observed R−S−M angles of ∼108−113°, one of the two remaining S p orbitals is used for a pseudo-σ-bond to the metal and the second for a π-bond to the metal (Chart 1). This symmetry reduction does not affect the relationship between pre-edge intensity and covalency. Thus, the equations in Table 2 still apply but with c_2 and c_3 modified to reflect one π-interaction per ligand.[14]

The spectra in Figure 5B exhibit a well-resolved pre-edge peak for Cu^{II} and Ni^{II}, a shoulder in the case of Co^{II}, and a pre-edge peak, which is shifted under the rising edge, for Fe^{II} and Mn^{II}. In the latter two cases, the energy of the pre-edge transition can be determined from the second derivative of the spectra. The Fe^{III} spectrum exhibits a very strong peak shifted to lower energy by 1.2

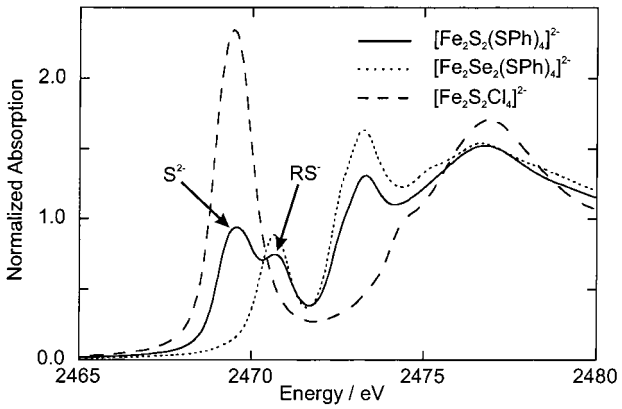

FIGURE 6. S K-edge XAS spectra of binuclear ferric Fe−S clusters.[15]

eV compared to that of Fe^{II}. The trend in the pre-edge transitions of the thiolates (Figure 5B) being closer to the edge transitions than those of the chlorides (Figure 5A) indicates a lower d manifold binding energy for the thiolate complexes. This is in agreement with the increased charge donor ability of thiolate vs chloride ligands (i.e., more covalent, vide infra), leading to a lower Z^{eff} on the metal.

The fitted intensities for the thiolate complexes can be converted to covalencies (Table 3) using plastocyanin as a reference (38% S 3p character in the HOMO). As expected, the covalency values are roughly twice as big as in the chloride complexes. The 3p valence orbitals of thiolate are higher in energy than the 3p orbitals of chloride, leading to a smaller energy gap to the metal d orbitals. In addition, the lower Z^{eff} leads to more diffuse orbitals and therefore better ligand−metal overlap. For $[Fe^{III}(SPh)_4]^-$, this gives 154% total covalency or 38.4% per Fe^{III}−SPh bond.

2.6. Bridging Sulfides. To extend this methodology to the dimeric Fe−S clusters in Figure 1, both bridging sulfides and terminal thiolates need to be considered. Figure 6 shows the S K-edge XAS spectrum of $[Fe^{III}_2S_2(SPh)_4]^{2-}$ (solid line). It exhibits two resolved pre-edge features, at 2469.5 and 2470.7 eV. Substituting the bridging sulfides by selenides, so that the only sulfur present is in the thiolate ligands, yields a spectrum (dotted line) with only one pre-edge feature at 2470.7 eV, which matches the high-energy feature of the $[Fe^{III}_2S_2(SPh)_4]^{2-}$ spectrum. Substitution of the terminal thiolates by chlorides yields a compound having only μ_2-sulfide bridges, and the spectrum (dashed line) shows only one pre-edge peak at 2469.5 eV, which coincides with the lower energy pre-edge feature of $[Fe^{III}_2S_2(SPh)_4]^{2-}$.[15] The lower energy pre-edge is therefore assigned to the bridging sulfide and the higher energy pre-edge feature to the terminal thiolate ligand. The magnitude of energy separation is due to the large difference in Z^{eff} of sulfide versus thiolate.

The fitted thiolate intensity can be converted into covalency as described in section 2.5 (29.7% per Fe^{III}−SPh bond), whereas a reference has to be developed for sulfide ligands. For this purpose we used $CsFeS_2$, which consists of a linear chain of tetrahedrally coordinated Fe^{III} ions bridged by two μ_2-sulfides, as in $[Fe^{III}_2S_2(SPh)_4]^{2-}$. The covalency of $CsFeS_2$ was independently estimated through analysis of $2P_{3/2}$ XPS spectra. This procedure yields a total covalency over the five half-occupied orbitals in $KFeS_2$ of 210%, or 52.5% per Fe−S bond.[15] The comparison shows that a bridging sulfide ligand is a factor of 2−3 more covalent than a terminal thiolate, as is expected from the low valence ionization energy and the extended radial distribution of S^{2-} relative to RS^- valence orbitals.

It is interesting to compare the covalencies of the monomeric and dimeric complexes as presented above for the copper compounds. The substitution of two thiolates in $[Fe^{III}(SPh)_4]^-$ with two bridging sulfides to form $[Fe^{III}_2S_2(SPh)_4]^{2-}$ reduces the covalency of the terminal thiolate from ∼38% per Fe−SPh bond in the monomer to ∼30% per Fe−SPh bond in the dimer. The sulfide ligands are stronger donors and reduce the charge donation of the remaining thiolates. These terminal thiolate ligands therefore serve as spectator ligands, probing the electron density on the iron center (see section 2.3.). In contrast, substitution of two strongly donating bridging sulfides by two weaker donating thiolates, i.e., on going from $CsFeS_2$ to $[Fe^{III}_2S_2(SPh)_4]^{2-}$, leads to increased covalency of the two remaining sulfides (55.5% per Fe−S bond in the chain compound to ∼72% in the dimer).

3. Applications

The methodology presented above allows one to experimentally determine the covalent interaction of chloride- and sulfur-containing ligands with transition metal centers possessing one or more holes in the d manifold. Covalency references for chloride, thiolate, and sulfide have been established, and molecules can be analyzed which have more than one type of ligand. We now apply this methodology to a number of longstanding questions in coordination and bioinorganic chemistry.

3.1. Blue Cu Sites: Covalency and ET Pathways. The blue Cu electron-transfer proteins (Figure 1) exhibit unique spectral features compared to those of normal, tetragonal Cu^{II} complexes: an unusually small parallel hyperfine splitting and a very intense absorption band at ∼600 nm.[16,17]

S K-edge XAS spectra of the blue Cu site in plastocyanin and a model compound $[Cu^{II}(tet\ b)(o\text{-}SC_6H_4CO_2)]$, having normal spectral features, show well-resolved pre-edge features (Figure 7A).[18] The appropriate renormalized intensity of plastocyanin is larger than that in the tet *b* model compound by nearly a factor of 3. Quantitative analysis of the intensity of these pre-edge peaks in Figure 7A yields 15% S p character in the HOMO of the model compound, whereas the cysteine ligand in plastocyanin has 38% character in the HOMO. Thus, the copper−cysteine bond in blue Cu is very covalent. This high covalency delocalizes a large amount of spin density onto the cysteine ligand, resulting in a smaller interaction of the spin density with the nuclear spin of the copper center, which is the origin of the small copper hyperfine coupling in blue Cu centers. This strong covalent bond also leads

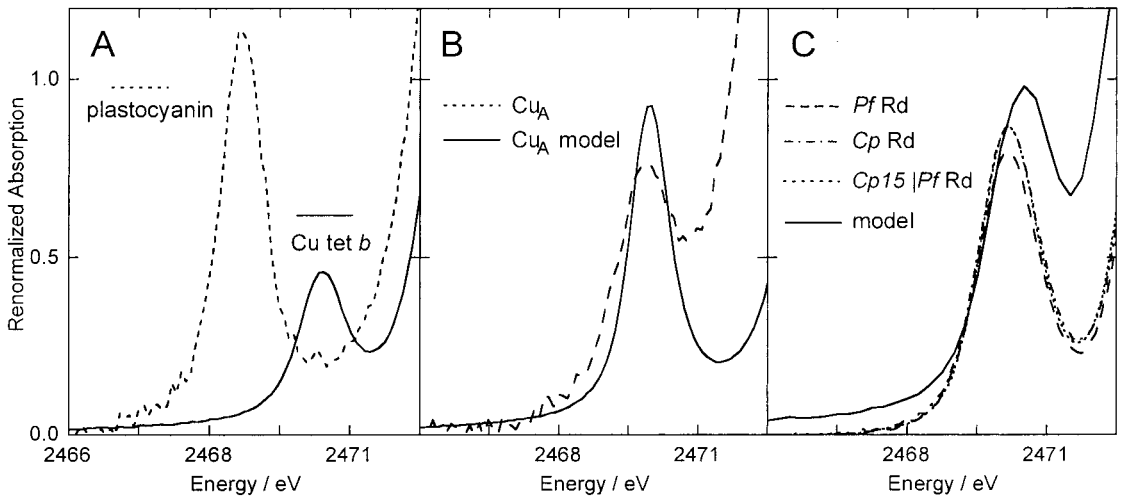

FIGURE 7. (A) S K-edge XAS spectra of $[Cu^{II}(tet\ b)(o\text{-}SC_6H_4CO_2)]$ (solid line) and plastocyanin (dashed line).[18] (B) S K-edge XAS spectra of $[(L^{iPrdacoS}Cu)_2]^+$ (solid line) and Cu_A construct from *Pseudomonas aeuginosa* (dashed line).[21,22] (C) S K-edge XAS spectra of $[Fe^{III}(S_2\text{-}o\text{-}xyl)_2]^-$ (solid line) and rubredoxins (broken lines).[23]

to an intense low-energy π-CT transition which corresponds to the 600 nm absorption band.

The high covalency of the blue Cu site provides strong electronic coupling (H_{DA}) into specific protein pathways for rapid long-range ET. Since the ET rate, k_{ET}, depends quadratically on H_{DA},[19] the large anisotropic CysS covalency in the blue Cu center can dramatically affect ET rates.[20] The large covalent interaction of the Cu $3d_{x^2-y^2}$ orbital with the thiolate π orbital produces a very efficient hole superexchange mechanism for rapid ET through a Cys-Tyr pathway in plastocyanin (or a Cys-His pathway in the multicopper oxidases and nitrite reductases[16,17]) to a remote site ~13 Å from the blue Cu center. Thus, S K-edge XAS demonstrates the presence of a highly covalent $Cu^{II}-S_{Cys}$ bond, which is of importance for rapid, long-range electron transfer.

3.2. The Cu_A Center: Electron Delocalization in Mixed-Valence Systems. The Cu_A electron-transfer site is comprised of a copper dimer bridged by two cysteine sulfurs (Figure 1). The Cu−Cu distance is very short (~2.44 Å). The electron-transfer process involves the $Cu^{1.5+}Cu^{1.5+}/Cu^+Cu^+$ redox couple. It was found from Cu hyperfine coupling that the mixed-valence form is delocalized.[16,17] Model compounds with a larger Cu−Cu separation of ~2.9 Å are also delocalized in the mixed-valence oxidation state. From combined absorption/MCD studies, the electronic coupling matrix elements H_{AB} of Cu_A and the model complex were found to be very different: $2H_{AB} \simeq 13\,000$ cm^{-1} for Cu_A and $2H_{AB} \simeq 5600$ cm^{-1} for the model. Here, H_{AB} is a measure of the interaction between the $3d_{x^2-y^2}$ orbitals on the two Cu centers in the dimer.

S K-edge XAS spectra of the mixed-valence forms of Cu_A and the model complex exhibit pre-edge features due to a transition to the half-occupied delocalized HOMO which are nearly equal in intensity (Figure 7B).[21,22] Thus, the covalent interactions between the Cu ions and the bridging thiolates in Cu_A and the model are of similar magnitudes. The similar pre-edge intensity in Figure 7B rules out superexchange as the origin for the difference in H_{AB}. The large value of H_{AB} for Cu_A must therefore be due to a direct overlap of the two d orbitals via a Cu−Cu bond. This derives from the difference in ligand field which rotates the valence d orbitals on the two coppers in the protein vs the model and gives σ orbital overlap. This metal−metal bond contribution to H_{AB} greatly stabilizes electron delocalization, even in the low-symmetry protein sites. This strong delocalization will contribute to the redox properties of the Cu_A site. The presence of the second Cu ion reduces $E°$, and valence delocalization leads to a reduction in the inner-sphere reorganization energy. Additionally, the high covalency of the bridging cysteines will enhance superexchange pathways for electron transfer into and out of Cu_A. Thus, the presence of a Cu−Cu bond in Cu_A, which maintains a delocalized ground state in the protein, should be functionally significant.

3.3. Rubredoxins and Ferredoxins: Hydrogen Bonding Effects. Fe−S-containing active sites are present in all forms of life and are very commonly involved in electron transfer. Rubredoxins are comprised of a monomeric Fe center ligated by four cysteine sulfurs. In 2Fe-ferredoxins, two Fe centers are bridged by two μ_2-sulfide ions and each Fe has two additional terminal cysteine ligands (Figure 1, see also section 2.6.). Rubredoxins operate between the Fe^{III}/Fe^{II} redox couple and 2Fe-ferredoxins between the $Fe^{III}Fe^{III}/Fe^{III}Fe^{II}$ redox couple. The reduction potentials of the active sites in proteins and model compounds are very different. Several contributions to the reduction potential due to the protein matrix are generally considered: charge interactions in the vicinity of the active site, contributions from the dielectric medium, and hydrogen bonding. Whereas the first two contributions should not influence the covalency of the iron−sulfur bond, hydrogen bonding to the sulfur reduces its charge donation to the iron. As shown above, variation of the ligand charge donation leads to a change of the energies of the redox-active orbital and, hence, to the reduction potential. Ligand K-edge XAS spectroscopy as a probe of ligand−metal covalency is thus a method of

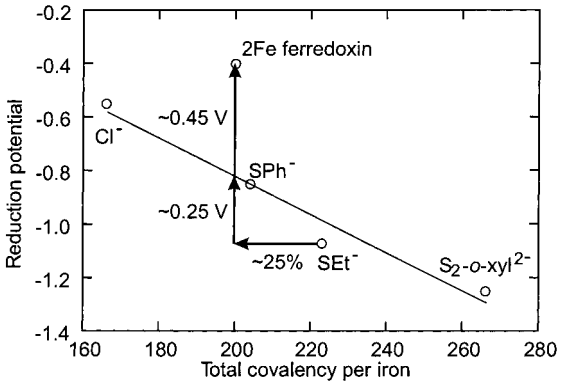

FIGURE 8. Correlation of the reduction potentials and total covalencies for $[Fe^{III}_2S_2(X)_4]^{2-}$, with X = Cl, SPh, SEt, and S_2-*o*-xyl. Included is the 2Fe ferredoxin from spinach.[25]

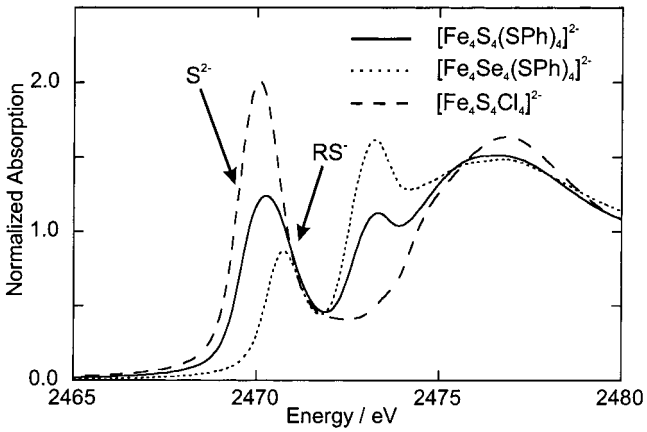

FIGURE 9. S K-edge XAS spectra of tetranuclear mixed-valence Fe−S clusters.[28]

choice in determining whether hydrogen bonds in the protein can affect the charge donation of the sulfur ligands and contribute to $E°$.

The reduction potential of various rubredoxins range from −60 to +5 mV vs SHE, whereas those of model complexes are in the region around −1 V vs SHE. Figure 7C shows the renormalized S K-edge spectra of three rubredoxins and a model compound, $[Fe^{III}(o\text{-}(SCH_2)_2\text{-}C_6H_4)_2]^-$.[23] The pre-edge feature of the model is more intense, and fitting gives a total covalency, i.e., the charge donation of the four ligands to the five half-occupied d orbitals, of ~171% for the model compound and ~143%, ~153%, and ~146% for the three different rubredoxins. The most significant structural difference between the model and protein sites is that the model site does not contain hydrogen bonds, whereas all three protein sites have six N−H···S hydrogen bonds from backbone donors to the cysteine sulfur. The reduced covalency of the proteins compared to that of the model compound can therefore be correlated with the presence of the hydrogen bonding in the proteins and should contribute to the increase in the reduction potentials.[24]

The reduction potentials of ferredoxin I from *Spinacia oleracea*, which is a 2Fe ferredoxin, and the model compound, $[Fe^{III}_2S_2(SEt)_4]^{2-}$, differ by 0.67 V. There are a number of hydrogen bonds to the thiolate and sulfide ligands in the protein. As with the rubredoxins, the S pre-edge intensity of the ferredoxin is reduced in comparison to that of the model compound, yielding a total covalency to the five d orbitals per Fe site in the protein of 200% compared to 223% for the model. Figure 8 shows the correlation of the reduction potentials of [2Fe-2S] models having different terminal ligands with their total covalency per iron. An increase in total covalency yields a lower reduction potential, which is expected due to the increase in energy of the redox-active orbital. Including ferredoxin on the graph in Figure 8[25] shows that the reduction of the total covalency by about 25% due to H-bonding gives ~0.25 V of the 0.67 V reduction potential difference. The remaining ~0.45 V must therefore be due to electrostatic effects in the protein pocket.

3.5. Fe−S Cluster: Localization vs Delocalization. The electronic structures of oligonuclear Fe−S clusters (Figure 1) has been studied by a variety of spectroscopic techniques.[26] In the binuclear $[2Fe\text{-}2S]^{2+,+}$ clusters, the iron centers are antiferromagnetically coupled in both the homovalent and mixed-valence states. The mixed-valence form exhibits localized Fe^{II} and Fe^{III} valencies. In contrast, in the mixed-valence $[4Fe\text{-}4S]^{2+}$ cubane clusters, which contain formally two Fe^{III} and two Fe^{II}, the valencies are delocalized over a pair of iron centers, yielding two mixed-valent $Fe^{2.5}_2$ pairs. The electron delocalization in the mixed-valence dimers leads to a ferromagnetically $S^* = {}^9/_2$ dimer subspin. The phenomenon of spin alignment in delocalized mixed-valence dimers is explained by a double exchange mechanism.[27]

We wish to understand the physical basis for localization and antiferromagnetic coupling in the mixed-valent $[2Fe\text{-}2S]^+$ and delocalization and ferromagnetic coupling in the $[4Fe\text{-}4S]^{2+}$ clusters. As can be seen from Figure 1, going from [2Fe-2S] to [4Fe-4S] involves replacing one thiolate on each Fe with the bridging sulfides of a second dimer, resulting in the formation of μ_3-sulfide bridges in the tetramers as compared to μ_2-sulfide bridges in the dimers. S K-edge XAS can be used to determine changes in bonding which occur between the dimer and tetramer that could affect delocalization. The S K-edge spectra for $[Fe_4S_4(SPh)_4]^{2-}$, $[Fe_4S_4Cl_4]^{2-}$, and $[Fe_4Se_4(SPh)_4]^{2-}$ are shown in Figure 9.[28] In comparison to the dimer spectra in Figure 6, the sulfide peak has shifted to higher energy so that the pre-edge transitions of the thiolate and the sulfide are no longer resolved.

Two major differences affect the energies and intensities of the pre-edges of $[Fe^{2.5}_4S_4(SPh)_4]^{2-}$ relative to those of $[Fe^{III}_2S_2(SR)_4]^{2-}$: (1) the formal oxidation state change from +2.5 to +3 and (2) the sulfide change from a μ_2- to a μ_3-bridging mode. To independently evaluate the changes associated only with the bridging mode and to define differences in the electronic structure that could contribute to delocalization in the tetramer, we compare the pre-edge of $[Fe^{2.5}_4S_4X_4]^{2-}$ to that of a hypothetical delocalized mixed-valence μ_2-sulfide dimer $[Fe^{2.5}_2S_2X_4]^{3-}$ which could be estimated from the experimental K-edge spectra of related compounds. Figure 10 (bold lines) gives the results for the X = Cl edges in $[Fe^{2.5}_4S_4Cl_4]^{2-}$ and the hypothetical

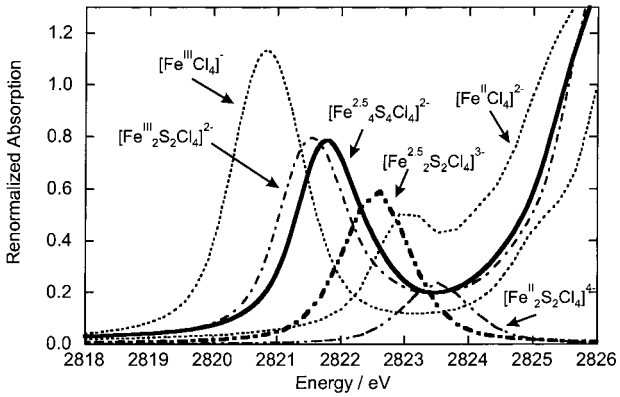

FIGURE 10. Cl K-edge XAS spectra of $[Fe^{II}Cl_4]^{2-}$, $[Fe^{III}Cl_4]^{-}$, $[Fe^{III}{}_2S_2Cl_4]^{2-}$, and $[Fe^{2.5}{}_4S_4Cl_4]^{2-}$, and the theoretical spectra of the hypothetical compounds $[Fe^{II}{}_2S_2Cl_4]^{4-}$ and $[Fe^{2.5}{}_2S_2Cl_4]^{3-}$ (see text).[28]

$[Fe^{2.5}{}_2S_2Cl_4]^{3-}$ dimer, which was estimated as follows.[28] Comparison of the pre-edge of $[Fe^{III}Cl_4]^{-}$ with that of $[Fe^{III}{}_2S_2Cl_4]^{2-}$ gives the effects of replacing two chlorides with two μ_2-sulfides. This can be used in combination with trends of energy and covalency changes obtained from density functional calculations to estimate the Cl pre-edge feature of $[Fe^{II}{}_2S_2Cl_4]^{4-}$ from that of $[Fe^{II}Cl_4]^{2-}$, which is observed experimentally. The average of the energies and intensities of the $[Fe^{III}{}_2S_2Cl_4]^{2-}$ and $[Fe^{II}{}_2S_2Cl_4]^{4-}$ pre-edge features then gives the predicted spectrum of the hypothetical $[Fe^{2.5}{}_2S_2Cl_4]^{3-}$-delocalized μ_2-sulfide-bridged dimer.[28] From Figure 10, the intensity of the terminal chloride in the tetramer is increased compared to that in the dimer, indicating more charge donation of the chloride to the iron center in the tetramer. Using the terminal chloride as a spectator ligand (vide supra), the bridging sulfides in the tetramers are weaker donors than those in the dimer. The lower pre-edge energy in the tetramer indicates a higher Z^{eff} of the iron in the tetramer due to the reduced total charge donation. Parallel analyses have been performed for the terminal thiolates and the bridging sulfides in the selenide- and chloride-substituted compounds. The main result is that the μ_3-sulfides in the tetranuclear cluster are much poorer donors per metal−ligand bond than the μ_2-sulfides in the dimer.[28]

For the [2Fe-2S] centers, it has been found that there is a large antiferromagnetic coupling present due to the μ_2-sulfide bridges that opposes electron delocalization. Antiferromagnetic coupling is dependent on the covalency of the bridging ligands. Thus, the reduced covalency of a μ_3-sulfide in the [4Fe-4S] centers should lead to a reduced antiferromagnetic coupling, favoring electron delocalization. A quantitative evaluation of these effects with the inclusion of vibronic coupling has been performed.[28]

4. Future Directions

The above studies demonstrate the power of S K-edge spectroscopy for the study of Fe−S clusters. We are currently extending these studies to the [4Fe-4S] cluster in HIPIP and 4Fe ferredoxins to evaluate hydrogen-bonding contributions to the ~1 eV difference in potentials between these classes of clusters. These studies will also be extended to the different oxidation states of the [4Fe-4S] clusters and the [3Fe-4S] cluster, which has both μ_2- and μ_3-bridging sulfides, to the effects of heterometal substitution into these clusters [M-3Fe-4S], and ultimately to the heterometal clusters in biology, in particular the FeMoco in nitrogenase.

There are also many other areas of biology where the covalency of sulfur ligation plays a central role in activating a metal site for catalysis (dithiolene−Mo bonding in oxo transferases, thiolate−heme Fe bonding in P450, etc.), and S K-edge studies should provide new insight into this key contribution to reactivity.

This research is supported by the NSF (Grants CHE-99805490, E.I.S., and CHE-9423181, K.O.H.) and the NIH (Grant RR-01209, K.O.H.). SSRL operations are funded by the U.S. Department of Energy, Office of Basic Energy Sciences. The Structural Molecular Biology Program is supported by the National Institutes of Health, National Center for Research Resources, Biomedical Technology Program and the Department of Energy, Office of Biological and Enviromental Research. T.G. thanks the Deutsche Forschungsgemeinschaft for a postdoctoral fellowship. We gratefully acknowledge the contributions of our co-workers and collaborators, who are cited in the referenced publications.

References

(1) Holm, R. H.; Kennepohl, P.; Solomon, E. I. Structural and Functional Aspects of Metal Sites in Biology. *Chem. Rev.* **1996**, *96*, 2239−2314.
(2) Li, J.; Noodleman, L.; Case, D. A. In *Inorganic Electronic Structure and Spectroscopy*; Solomon, E. I., Lever, A. B. P., Eds.; John Wiley & Sons: New York, 1999; Vol. I, pp 661−724.
(3) Solomon, E. I. Inorganic Spectroscopy−An Overview. *Comments Inorg. Chem.* **1984**, *3*, 227−320.
(4) Solomon, E. I.; Hanson, M. In *Inorganic Electronic Structure and Spectroscopy*; Solomon, E. I., Lever, A. B. P., Eds.; John Wiley & Sons: New York, 1999; Vol. II, pp 1−130.
(5) Hedman, B.; Hodgson, K. O.; Solomon, E. I. X-Ray Absorption-Edge Spectroscopy of Ligands Bound to Open-Shell Metal-Ions: Chlorine K-Edge Studies of Covalency in $CuCl_4^{2-}$. *J. Am. Chem. Soc.* **1990**, *112*, 1643−1645.
(6) Neese, F.; Hedman, B.; Hodgson, K. O.; Solomon, E. I. Relationship between the Dipole Strength of Ligand Pre-edge Transitions and Metal−Ligand Covalency. *Inorg. Chem.* **1999**, *38*, 4854−4860.
(7) Shadle, S. E.; Hedman, B.; Hodgson, K. O.; Solomon, E. I. Ligand K-Edge X-ray Absorption Spectroscopic Studies: Metal−Ligand Covalency in a Series of Transition Metal Tetrachlorides. *J. Am. Chem. Soc.* **1995**, *117*, 2259−2272.
(8) van der Laan, G.; Westra, C.; Haas, C.; Sawatzky, G. A. Satellite Structure in Photoelectron and Auger Spectra of Copper Dihalides. *Phys. Rev. B* **1981**, *23*, 4369−4380.
(9) Kau, L. S.; Spira-Solomon, D. J.; Penner-Hahn, J. E.; Hodgson, K. O.; Solomon, E. I. X-ray Absorption Edge Determination of the Oxidation State and Coordination Number of Copper: Application to the Type-3 Site in *Rhus vernicifera* Laccase and Its Reaction with Oxygen. *J. Am. Chem. Soc.* **1987**, *109*, 6433−6442.
(10) Shadle, S. E.; Hedman, B.; Hodgson, K. O.; Solomon, E. I. Ligand K-edge X-ray Absorption Spectroscopy as a Probe of Ligand−Metal Bonding: Charge Donation and Covalency in Copper-Chloride Systems. *Inorg. Chem.* **1994**, *33*, 4235−4244.
(11) The energies reported for the rising edge positions were determined from the highest energy maximum in the first derivative of the data in the rising edge region.
(12) Note that the measured intensities are normalized intensities and depend on the choice of the normalization energy for the edge-jump. Since the final state contains the wave function of the outgoing photoelectron and the photoionization cross section is dependent on the photon energy, the numerical values of the transition moment integrals have no direct physical interpretation. They can be compared for the same ligand type using the same

normalization procedure, but they cannot be compared between different ligand types.

(13) Izumi, Y.; Glaser, T.; Rose, K.; McMaster, J.; Basu, P.; Enemark, J. H.; Hedman, B.; Hodgson, K. O.; Solomon, E. I. Ligand K-Edge and Metal L-Edge X-ray Absorption Spectroscopy and Density Functional Calculations of Oxomolybdenum Complexes with Thiolate and Related Ligands: Implications for Sulfite Oxidase. *J. Am. Chem. Soc.* **1999**, *121*, 10035−10046.

(14) Rose Williams, K.; Hedman, B.; Hodgson, K. O.; Solomon, E. I. Ligand K-Edge X-ray Absorption Spectroscopic Studies: Metal−Ligand Covalency in Transition Metal Tetrathiolates. *Inorg. Chim. Acta* **1997**, *263*, 315−321.

(15) Rose, K.; Shadle, S. E.; Glaser, T.; de Vries, S.; Cherepanow, A.; Canters, G. W.; Hedman, B.; Hodgson, K. O.; Solomon, E. I. Investigation of the Electronic Structure of 2Fe-2S Model Complexes and the Rieske Protein Using Ligand K-Edge X-ray Absorption Spectroscopy. *J. Am. Chem. Soc.* **1999**, *121*, 2353−2363.

(16) Randall, D. W.; Gamelin, D. R.; LaCroix, L. B.; Solomon, E. I. Electronic Structure Contributions to Electron Transfer in Blue Cu and Cu_A. *J. Biol. Inorg. Chem.* **2000**, *5*, 16−29.

(17) Solomon, E. I.; Randall, D. W.; Glaser, T. Electronic Structures of Active Sites in Electron Transfer Metalloproteins: Contributions to Reactivity. *Coord. Chem. Rev.* **2000**, *200*, 595−632.

(18) Shadle, S. E.; Penner-Hahn, J. E.; Schugar, H. J.; Hedman, B.; Hodgson, K. O.; Solomon, E. I. X-ray Absorption Spectroscopic Studies of the Blue Copper Site: Metal and Ligand K-edge Studies to Probe the Origin of the EPR Hyperfine Splitting in Plastocyanin. *J. Am. Chem. Soc.* **1993**, *115*, 767−776.

(19) Marcus, R. A.; Sutin, N. Electron Transfers in Chemistry and Biology. *Biochim. Biophys. Acta* **1985**, *811*, 265−322.

(20) Lowery, M. D.; Guckert, J. A.; Gebhard, M. S.; Solomon, E. I. Active-Site Electronic-Structure Contributions to Electron-Transfer Pathways in Rubredoxin and Plastocyanin: Direct Versus Superexchange. *J. Am. Chem. Soc.* **1993**, *115*, 3012−3013.

(21) Rose Williams, K.; Gamelin, D. R.; LaCroix, L. B.; Houser, R. P.; Tolman, W. B.; Mulder, T. C.; de Vries, S.; Hedman, B.; Hodgson, K. O.; Solomon, E. I. Influence of Copper−Sulfur Covalency and Copper−Copper Bonding on Valence Delocalization and Electron-Transfer in the Cu_A Site of Cytochrome *c* Oxidase. *J. Am. Chem. Soc.* **1997**, *119*, 613−614.

(22) DeBeer, S.; Hedman, B.; Hodgson, K. O.; Solomon, E. I., unpublished results.

(23) Rose, K.; Shadle, S. E.; Eidsness, M. K.; Kurtz, D. M., Jr.; Scott, R. A.; Hedman, B.; Hodgson, K. O.; Solomon, E. I. Investigation of Iron−Sulfur Covalency in Rubredoxins and a Model System Using Sulfur K-edge X-ray Absorption Spectroscopy. *J. Am. Chem. Soc.* **1998**, *120*, 10743−10747.

(24) Note that the covalency of $[Fe(SR)_4]^-$ varies with the nature of R.

(25) Anxolabéhère-Mallart, E.; Glaser, T.; Frank, P.; Aliverti, A.; Zanetti, G.; Hedman, B.; Hodgson, K. O.; Solomon, E. I., manuscript in preparation.

(26) Beinert, H.; Holm, R. H.; Münck, E. Iron−Sulfur Clusters: Nature's Modular Multipurpose Structures. *Science* **1997**, *277*, 653−659.

(27) Blondin, G.; Girerd, J. J. Interplay of Electron Exchange and Electron-Transfer in Metal Polynuclear Complexes in Proteins or Chemical Models. *Chem. Rev.* **1990**, *90*, 1359−1376.

(28) Glaser, T.; Rose, K.; Shadle, S. E.; Hedman, B.; Hodgson, K. O.; Solomon, E. I. S K-Edge Absorption Studies of Tetranuclear Iron−Sulfur Clusters: μ-Sulfide Bonding and its Contribution to Electron Delocalization, *J. Am. Chem. Soc.,* submitted for publication.

(29) Gamelin, D. R.; Bominaar, E. L.; Kirk, M. L.; Wieghardt, K.; Solomon, E. I. Excited-State Contributions to Ground-State Properties of Mixed-Valence Dimers: Spectral and Electronic-Structural Studies of $[Fe_2(OH)_3(tmtacn)_2]^{2+}$ Related to the $[Fe_2S_2]^+$ Active-Sites of Plant-Type Ferredoxins. *J. Am. Chem. Soc.* **1996**, *118*, 8085−8097.

(30) Didziulis, S. V.; Cohen, S. L.; Gewirth, A. A.; Solomon, E. I. Variable Photon Energy Photoelectron Spectroscopic Studies of Copper Chlorides: an Experimental Probe of Metal−Ligand Bonding and Changes in Electronic-Structure on Ionization. *J. Am. Chem. Soc.* **1988**, *110*, 250−268.

(31) Gewirth, A. A.; Cohen, S. L.; Schugar, H. J.; Solomon, E. I. Spectroscopic and Theoretical-Studies of the Unusual Electron-Paramagnetic-Resonance Parameters of Distorted Tetrahedral Cupric Sites: Correlations to X-ray Spectral Features of Core Levels. *Inorg. Chem.* **1987**, *26*, 1133−1146.

(32) Cohen, S. L. Ph.D. Thesis, Massachusetts Institute of Technology, 1986.

AR990125C